ADVANCED OPTICAL MATERIALS
www.advopticalmat.de

Step Function in Momentum Space by a Metagrating

Mahmoud A. A. Abouelatta, Sergejs Boroviks, Olivier J. F. Martin, and Karim Achouri*

Metasurface research has shown significant potential for controlling the polarization, amplitude, phase, and propagation direction of light. Nevertheless, control over the angular response of incident light remains a long-standing problem. In this work, the potential of diffractive systems for obtaining a step function in momentum space is shown, where the mirror symmetry of the angular transmittance is broken. By engineering the scattering response of an asymmetric particle in a metagrating, such a step function can be obtained in a passive, reciprocal, and lossless fashion. More specifically, the metagrating performs filtering in momentum space with an abrupt switching from reflection to transmission for an incident electromagnetic wave with an arbitrary spatial profile. This metagrating may find diverse applications in optical spatial analog computing. Moreover, it paves the way for exploring the capabilities of diffractive systems for gaining full control over the angular response of light using arbitrary momentum transfer functions.

1. Introduction

Metasurfaces have enabled versatile ways to control the polarization, the temporal frequency response, the amplitude and the phase profiles of light. By engineering their electromagnetic response at the sub-wavelength scale, a plethora of metasurface concepts and applications have been proposed to manipulate these degrees of freedom.[1–3] However, despite the great light propagation engineering capabilities that metasurfaces enable, the possible options they offer for controlling the spatial frequency of light (i.e., to control the angular response) remain limited. Hence, most metasurface applications have been studied for a limited angular range of the input signal.[4,5] Achieving scattering control over the full angular spectrum would make spatial analog computing possible in ultra-compact systems where signals are processed at the speed of light, and are analyzed in the spatial Fourier domain.[6] In this area of research, several works have already shown the potential of metasurfaces for diverse applications such as spatial differentiation,[7] planar retro-reflection,[8] and refraction control,[9,10] among many others.[11,12] One of the milestones in the research associated with the angular response of light is the generalized laws of refraction and reflection,[13] which model how light may be deflected by the introduction of planar phase gradients.[14,15] However, a careful examination of these laws showed that they are merely an approximation to the diffraction theory,[16] which implies that they do not provide rigorous solutions to Maxwell's equations. Consequently, they cannot, for example, quantitatively describe the total efficiency of beam steering in a system[17] and do not allow for fully efficient refraction operations.[18] Conversely, the efficiency of beam steering was studied rigorously by effective medium theory[9,19] as well as diffraction theory.[20,21] This suggests that studies based on diffraction theory are of paramount importance to achieve an advanced control over the angular response of light.

Among the various challenges in angular light scattering control, breaking the symmetry of angular transmission through an optical system is particularly intriguing, as it corresponds to momentum-space filtering. This effect is highly relevant for applications such as optical computing, Schlieren imaging, and smart windows. In particular, for Schlieren imaging, realizing a step-function response in momentum space—with a sharp transition from transmission to reflection—is of paramount importance, as it replicates the action of a knife-edge placed at the focal plane in conventional free-space Schlieren systems. Several examples of asymmetric metasurfaces that break the angular symmetry of the transmittance have already been proposed. For instance, by sandwiching a metasurface between two polarizers and manipulating the incident polarization state, the angular symmetry of the optical transfer function may be broken.[22] A few other works have reported angularly asymmetric absorbance (A) by relying on the anomalous Brewster effect,[23] and evanescent field engineering via a phase-gradient (i.e., spatially-varying) metasurface.[24] It is important to note that all of these designs require, in one way or another, asymmetric angular losses in order to achieve asymmetric angular transmittance. This begs the question as to whether or not it is possible to achieve asymmetric angular transmittance in a lossless fashion. It turns out that, as we show thereafter, it is in fact impossible to achieve lossless

M. A. A. Abouelatta, K. Achouri
Laboratory for Advanced Electromagnetics and Photonics
École Polytechnique Fédérale de Lausanne (EPFL)
Lausanne 1015, Switzerland
E-mail: mahmoud.abouelatta@epfl.ch
S. Boroviks, O. J. F. Martin
Nanophotonics and Metrology Laboratory
École Polytechnique Fédérale de Lausanne (EPFL)
Lausanne 1015, Switzerland

The ORCID identification number(s) for the author(s) of this article can be found under https://doi.org/10.1002/adom.202500265

DOI: 10.1002/adom.202500265

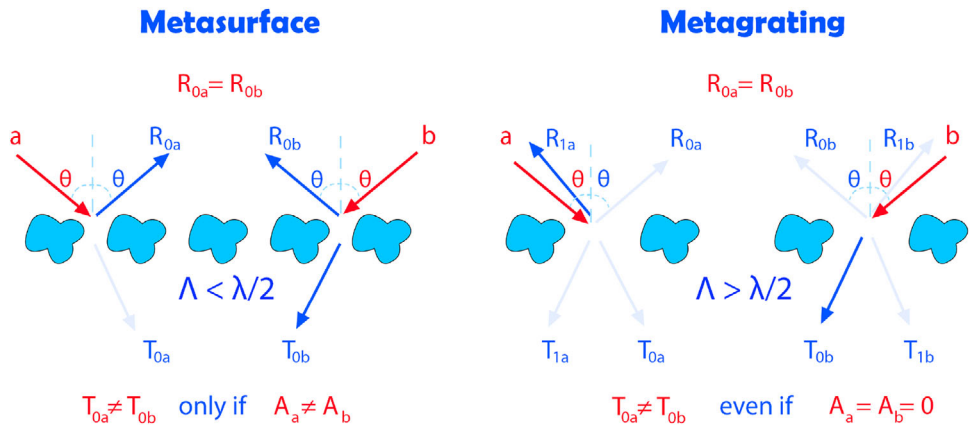

Figure 1. Illustration of the key differences between a non-diffractive (metasurface) and a diffractive array of scatterers (metagrating). Left side: the angular symmetry of the 0th-order reflectance is enforced by reciprocity, whereas the angular symmetry of the transmittance can be broken by introducing asymmetric absorbance ($A_a \neq A_b$). Right side: the angular symmetry of the transmittance is broken by allowing the system to be diffractive while engineering the 0th-order reflectance to have a value close to zero. R_{0a}, R_{1a}, T_{0a} and T_{1a} denote the 0th-order, first-order reflectance, 0th-order, and first-order transmittance, respectively, when a plane wave is incident from port "a," and similarly for waves incident from port "b." A_a and A_b represent the absorbance for incidence from port "a" and "b," respectively, while Λ is the array period.

asymmetric amplitude for the angular transmittance with a planar non-diffractive reciprocal optical system.

To overcome this limitation, we shall therefore explore the potential of diffractive surfaces, e.g., metagratings, to achieve such an optical response. In contrast to non-diffractive uniform metasurfaces, metagratings have extra degrees of freedom for manipulating electromagnetic waves in multiple ports. As such, several metagrating schemes have been introduced in the literature for extreme beam steering,[20] parallel computing,[25] solving integral equations,[26] and spatiotemporal pulse shaping.[27–29]

In this work, we demonstrate how asymmetric angular transmittance may be theoretically achieved with a lossless reciprocal diffraction grating. We then proceed to fabricate such a device and experimentally verify its asymmetric scattering properties. We anticipate that asymmetric transmittance may find applications in optical analog signal processing devices, for instance, to achieve image filtering in an ultra-thin miniaturized fashion. A typical example would be that of a Schlieren imaging system, which relies on the concept of filtering out a part of the momentum space with a knife edge, that may be implemented without a bulky free-space system composed of multiple lenses or mirrors. It could also span further applications such as angular dependent smart windows where the Sun's energy needs to be reflected for a desired angular range (instead of being absorbed by the system).[30] Moreover, the approach used in this work could inspire future studies for manipulating the spatial Fourier space in novel ways, paving the way for ultra-compact angular filters or unprecedented momentum transfer functions.

Note that our proposed concept is clearly different than that of conventional blazed grating structures since the latter are engineered to redirect the incident power into a desired diffraction order, whereas our metagrating is optimized to maximize the transmission asymmetry for both positive and negative incidence angles.

2. Theoretical Considerations

The underlying principle of how angular asymmetry has been previously achieved using non-diffractive metasurface platforms is illustrated on the left side of **Figure 1**.[23] Owing to the fact that the reciprocity of such systems enforces the reflectance (R) to have angular symmetry (i.e., $R(\theta) = R(-\theta)$), the *only* possible way to break the symmetry of the angular transmittance (i.e., $T(\theta) \neq T(-\theta)$) is by having angularly asymmetric absorption.[31] This is straightforward to demonstrate, by considering that

$$T(\theta) = 1 - R(\theta) - A(\theta) \quad \text{and} \quad T(-\theta) = 1 - R(-\theta) - A(-\theta), \quad (1)$$

which implies that $T(\theta) \neq T(-\theta)$ is only possible if $A(\theta) \neq A(-\theta)$.

The concept that we introduce in this work is shown on the right side of Figure 1. By allowing propagation in multiple diffraction directions (i.e., the 0th and 1st diffraction orders), and by appropriately breaking the spatial symmetry of the system, the angular transmittance may have an asymmetric response *without* enforcing the system to be dissipative. Additionally, to maximize this angular transmission asymmetry, and thus maximize the efficiency of the system, it is necessary to minimize the 0th-order reflectance, which is angularly symmetric by reciprocity, as explained above.

Thus far, we discussed the metagrating concept in the framework of the reciprocity theorem. We shall now illustrate it from the perspective of spatial symmetries. It is insightful to consider which kinds of symmetries may be preserved, and which ones should be broken, in order to achieve angular asymmetry around the z-axis, as illustrated on the right side of Figure 1. Such insights allow us to find the simplest possible structure for this purpose and provide a powerful approach to optimize the scattering response of the system. For example, a unit cell which has mirror symmetry (σ_x) and periodicity along the x-axis cannot have angular asymmetry around the normal direction (i.e., the z-axis). However, when it comes to mirror symmetry along

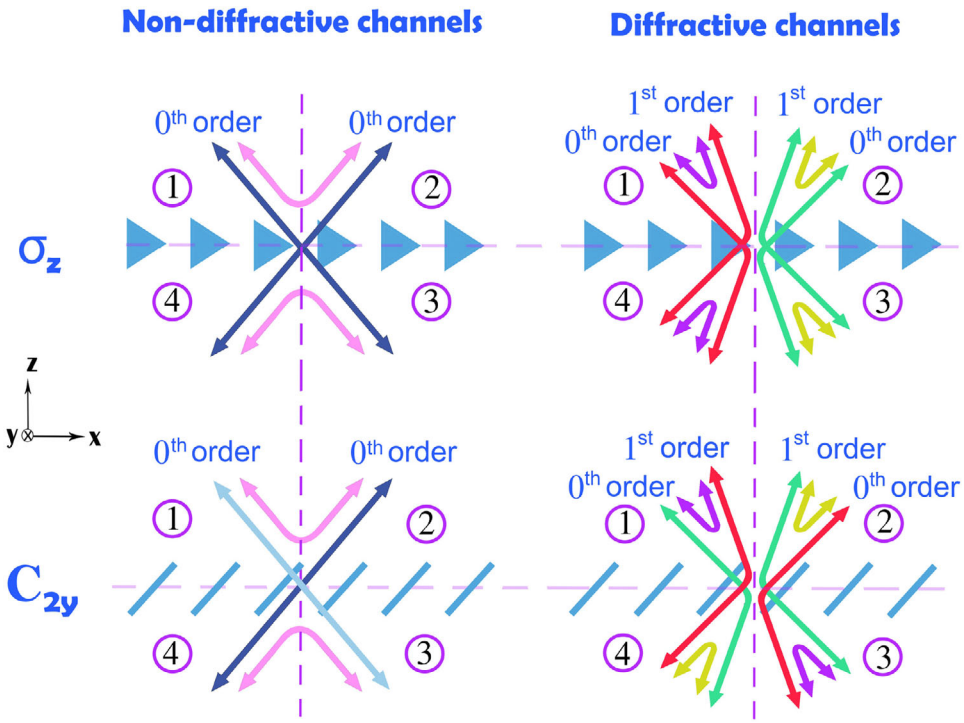

Figure 2. Non-diffractive and diffractive channels of wave propagation in systems with two different kinds of spatial symmetries. The top row corresponds to mirror symmetry in the direction of the *z*-axis (σ_z). The bottom row corresponds to rotation symmetry by 180° (C_{2y}) around the *y*-axis. The arrows in the figure represent the scattering between the different ports of the various quadrants and identical colors indicate identical scattering parameters. The arrows are double sided to visualize the reciprocity of the system in different scattering channels.

the *z*-axis (σ_z), the implications are more involved. For this reason, we have developed a formalism that allows us to easily and rigorously deduce the scattering symmetries in a diffraction grating (with one-dimensional periodicity) based on the spatial symmetries of its unit cell. This formalism is described in detail in Section S1 (Supporting Information). For an array that is infinite along the *y*-direction, the scattering symmetries corresponding to two different possible unit cell spatial symmetries, i.e., only possessing σ_z or C_{2y}, are illustrated in **Figure 2**. The formulas for the scattering matrices corresponding to σ_z and C_{2y} symmetries are shown in Eqs. (S9) and (S10), respectively. We consider that the incident wave is impinging on the array in the plane of symmetry (*xz*-plane) from quadrants denoted 1 to 4 at an arbitrary angle. On the left side of the figure, we show the scattering symmetries between the non-diffractive channels (0th order) whereas the right side of the figure shows the coupling between the 0th order channels and the 1st order diffractive channels.

As can be seen in the top-left of Figure 2, when a wave is incident from quadrant 1 to 3 or from quadrant 4 to 2, the 0th order transmittance has to be the same due to the mirror symmetry along the *z*-axis (σ_z). Reciprocity also enforces the transmittance from quadrant 4 to 2 and from quadrant 2 to 4 to be the same. Thus, considering these two results, the system has to be angularly symmetric for the 0th order transmittance demonstrating that a structure with only σ_z symmetry (and broken σ_x symmetry) *cannot* be used for angularly asymmetric transmittance in the 0th order. Nevertheless, rerouting the energy into the 1st order transmittance or reflectance may be angularly asymmetric, as shown in the upper right side of Figure 2.

In the case where the structure exhibits only a C_{2y} symmetry, symmetry breaking in both the 0th and 1st order transmittance channels is possible, as shown in the bottom-left of Figure 2. Additionally, the 1st order reflectance is also asymmetric, implying that a structure possessing C_{2y} symmetry is the simplest possible structure to achieve our desired asymmetric scattering response where the symmetries in both the 0th and 1st orders need to be simultaneously broken[32].

Besides reciprocity and symmetry perspectives, the metagrating could also be analyzed based on multipolar theory. We show the multipolar decomposition for a unit cell of the metagrating in Figure S7 (Supporting Information), which proves that our system could be modeled as an array of 2D tilted electric dipoles in the plane of symmetry (i.e., the *xz*-plane). Since the metagrating is composed of dipoles only, the nonlocal interactions between different unit cells are negligible, and consequently, the introduced metagrating's unit cell is local despite its strong angular dependence. In this context, a perspective article classifies metasurfaces into three categories (local nondiffractive metasurface, nonlocal nondiffractive metasurface, and nonlocal diffractive metasurface).[33] In contrast to these three categories, our metagrating could be regarded as a diffractive metasurface with unit cell harboring local field interactions. Thus demonstrating that spatial dispersion[34] (e.g., a nonlocal polarizability tensor) is not a prerequisite for achieving significant angular dispersion. In future work, we will show how such kind of systems composed of tilted dipoles could be analytically modeled using Floquet expansion and the polarizability tensor.

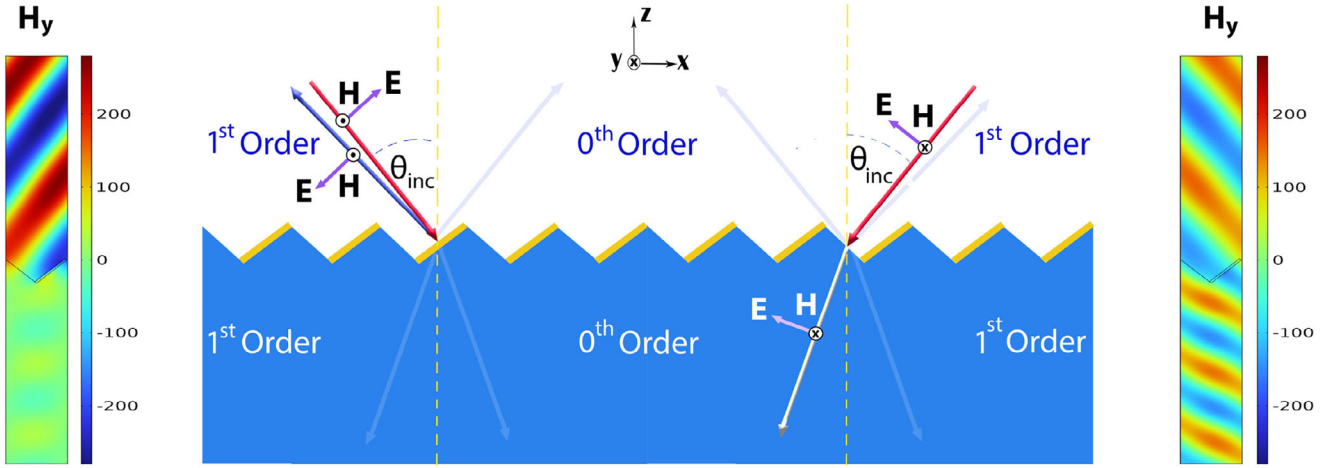

Figure 3. Metagrating with angular asymmetric transmittance. Two cases are depicted where two incident TM polarized plane waves are retroreflected and transmitted for positive and negative incidence angles, respectively. The metagrating consists of an array of silica ridges (shown in blue color) with asymmetrically deposited gold strips (shown in yellow color). The magnetic field profile (H_y) is shown on the left and right sides for two TM plane waves incident on the metagrating with angles equal to 55° and −55°, respectively. The wavelength of the incident TM waves for these two field profiles is equal to 900 nm. The period of the grating (Λ) is 525 nm, while the triangular ridges are tilted with respect to the *x*-axis with an angle equal to 41°. The thickness of the gold strips is 22 nm. The magnetic-field distributions were computed using COMSOL Multiphysics.

Based on the consideration of reciprocity and spatial symmetries, we come to the conclusion that, in order to achieve lossless, reciprocal, asymmetric angular transmittance, we should implement a diffraction grating with C_{2y} symmetry.

3. Numerical and Experimental Results

The schematic of the proposed metagrating is depicted in **Figure 3**. It consists of triangular ridges made of silica with a thin layer of gold deposited on only one side of these ridges. The metagrating fully transmits transverse magnetic (TM) plane waves having negative angles of incidence with respect to the *x*-axis (i.e., a negative *x*-component for the incident wave vector), as demonstrated by the magnetic field (H_y) distribution on the right side of Figure 3. However, the metagrating retro-reflects the incident TM plane waves which possess positive angles of incidence (i.e., from the left) where the energy is being rerouted into the first reflection diffraction order, as depicted in the magnetic field (H_y) distribution on the left side of Figure 3.

The 0th-order, 1st-order, and overall transmittance of the introduced metagrating are shown in **Figure 4**a–c, respectively, for a pair of incidence angles equal to −55° and 55°. A notable asymmetry between the two incidence angles in the 0th-order and overall transmittance is present for operation bandwidths ranging from 0.8 to 1.18 μm, and from 0.8 to 0.95 μm, respectively. The physical origin of such symmetry breaking is rooted in the scattering of the oblique gold strips, which is engineered to reflect the input energy into the 1st diffraction order for positive angles of incidence. The 0th-order, 1st-order, and overall reflectance of the metagrating are also shown in Figure 4d–f, respectively. Reciprocity theorem enforces the 0th-order reflectance to be symmetric as shown in Figure 4d. Nevertheless, the scattering response of the gold strips is optimized to minimize the specular reflectance. Consequently, the angular transmittance is remarkably asymmetric in the diffractive regime without imposing angularly asymmetric absorbance on the system.

To visualize the angular scattering behavior of the metagrating, we now study its response in Fourier space for spatial frequencies along both *x* and *y* axes. This means that the plane of incidence for the input TM plane waves is not restricted to the plane of translation symmetry (i.e., the *xz*-plane). Consequently, the directions of diffracted waves are no longer restricted to this plane either and, owing to momentum conservation, the locus of the diffraction orders becomes a conical surface. This phenomenon, known as conical diffraction, is typically studied by finding the exact solutions of the electromagnetic fields of an arbitrary grating based on Maxwell's equations.[35] Here, we consider a simpler alternative based on symmetry considerations (see a detailed discussion in Section S2, Supporting Information) to find the cutoff condition in Fourier space for each diffraction order to start propagating. The resulting condition is given by

$$\hat{k}_y^2 = \frac{n_o^2}{n_i^2} - \left(\hat{k}_x + \frac{m\lambda_0}{n_i\Lambda}\right)^2, \tag{2}$$

where $\hat{k}_x$ and $\hat{k}_y$ are the normalized components of the wave vector in the *x* and *y* directions, whereas Λ, λ_0, n_o, and n_i denote the grating period, the free-space wavelength, the input and output port refractive indices, respectively. **Figure 5**a depicts a unit cell of the proposed metagrating when the input wave is incident from air to silica. Figure 5b shows the total transmittance as a function of the incidence angle and the input wavelength for the case shown in Figure 5a. Note that there are four curves around which abrupt changes in transmittance occur. These curves denote the cutoff conditions for the first diffraction order in the reflection and transmission media, which are derived from the grating equation. Additionally, it can be seen that there is remarkable angular asymmetry in the total transmittance between negative

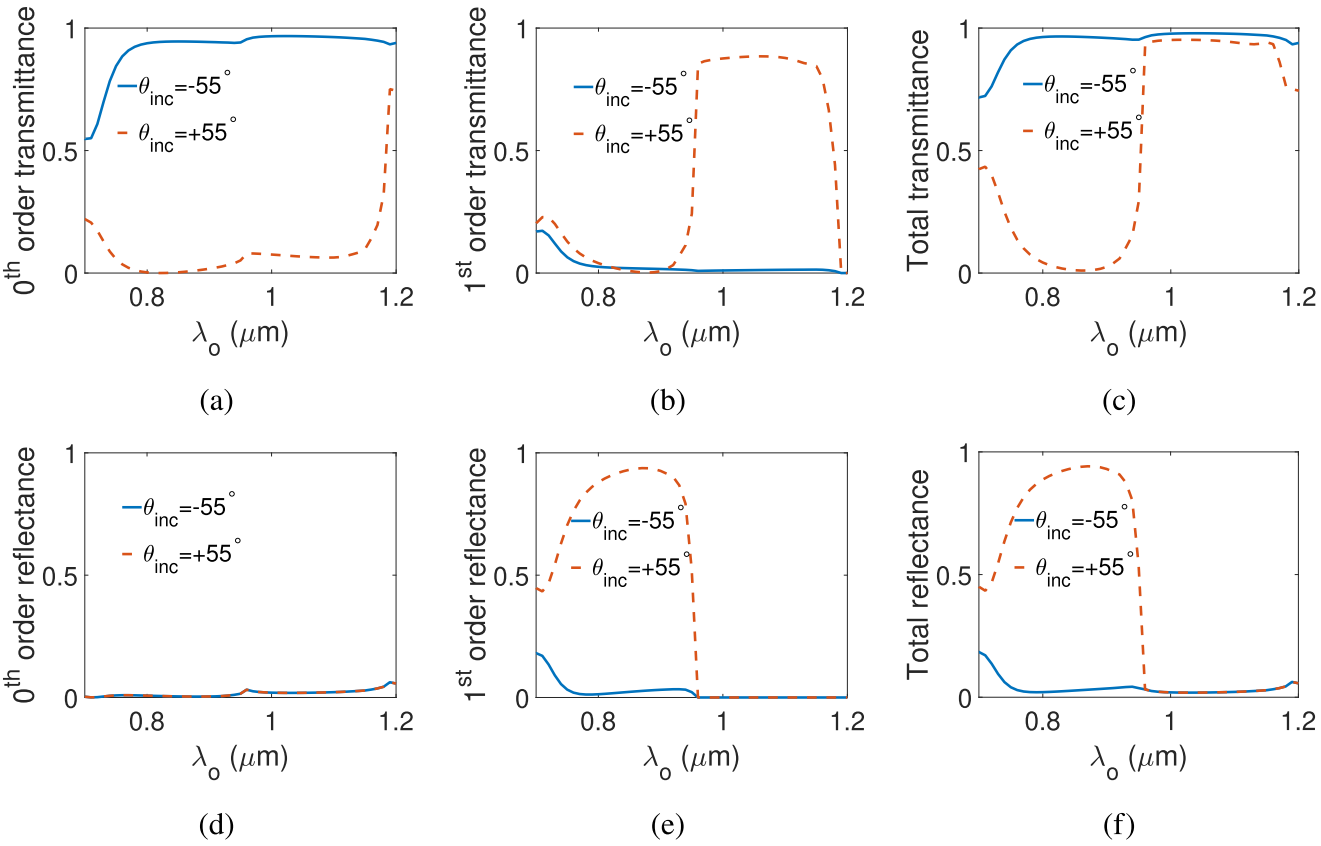

Figure 4. a) 0th-order, b) 1st-order, and c) overall transmittance of the introduced metagrating for two angles of incidence −55° and 55°. d) 0th-order, e) 1st-order, and f) overall reflectance.

and positive angles greater than roughly 40° spanning an operation bandwidth starting from 0.8 to 0.95 μm. For $\lambda_0 = 0.9\,\mu m$, the total transmittance is computed for all of the Fourier space as shown in Figure 5c. This is achieved by sampling a sphere representing all of the possible wave vector components for the incident plane wave, while computing the transmittance for every sample based on full-wave simulations. It can also be noted that there are four lines representing the cutoff conditions for the first diffraction order in transmission and reflection domains as described by Eq. (2). The total reflectance is shown in Figure 5d, indicating that the metagrating exhibits theoretically low absorption at this wavelength when combined with the total transmittance in Figure 5c (see Figure S6, Supporting Information). Step-function-like transitions from transmission to reflection in momentum space are evident in Figures 5c,d. Such abrupt transitions are highly beneficial for applications such as Schlieren imaging, as they are equivalent to the effect of a knife-edge placed at the focal plane of a free-space system, as discussed in the Introduction. While achieving such transitions is challenging in non-diffractive systems, they become possible here by engineering the angular scattering within each unit cell and leveraging Rayleigh anomalies associated with the cutoff conditions.

For comparison, we also consider another unit cell that is depicted in Figure 5e for the case when the reflection and transmission domains are both made of silica (gold strips embedded into silica). Figures 5f–h are analogous to Figures 5b–d, respectively, depicting the angular dispersion of the total transmittance, Fourier-space total transmittance, and reflectance as a function of the spatial frequencies in the x and y directions at a wavelength equal to $1.1\mu m$ for the unit cell shown in Figure 5e. Note that the physical difference between this unit cell and the one in Figure 5a is the fact that the cutoff conditions for the first diffraction order in the reflection and transmission regimes (i.e., the four curves in Figure 5b) merge in two curves leading to a broader range for angular asymmetry. This means that the angular range for asymmetry is mainly limited by the refractive index contrast between the incident and transmitted media, and it could be extended if the surrounding medium is homogeneous.

For both structures in Figures 5a and e, there is a minor amount of angular asymmetry in the non-diffractive regime. This can be explained by the fact that gold exhibits ohmic losses, which results in angularly asymmetric absorption ($A(\theta) \neq A(-\theta)$) due to the broken symmetry of the array.

We have fabricated and optically characterized a sample of the proposed metagrating structure with an area equal to 1 cm^2. The process flow for fabrication is described in the Section S6 (Supporting Information). The scanning electron microscope (SEM) image in **Figure 6a** shows a cross-sectional view of the fabricated sample (obtained using focused-ion-beam (FIB) milling), after thermal wet oxidation processing of silicon. Note that the interface between silicon and silica below the periodic array is smooth and non-diffractive. Moreover, the gold layer is

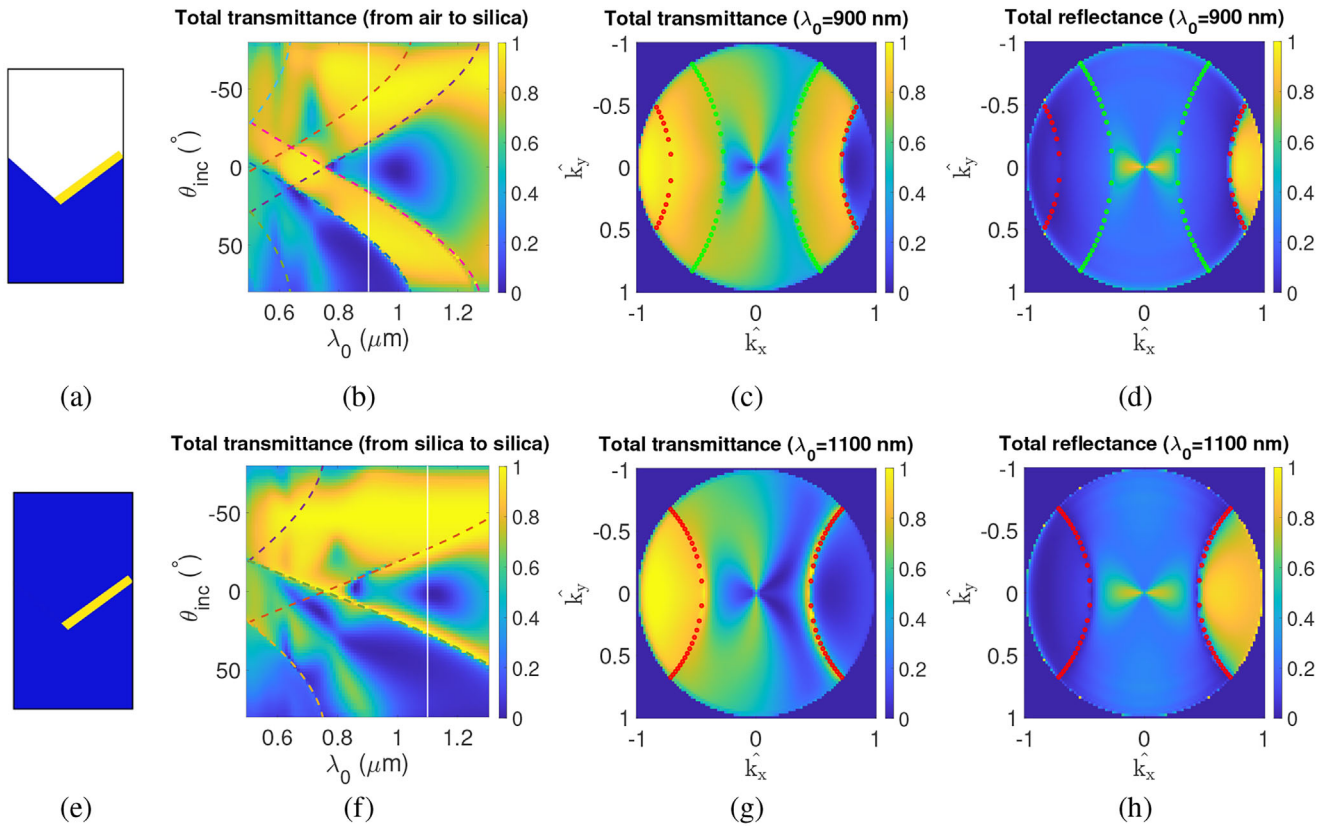

Figure 5. a) Schematic representing a case for incidence from air to silica. b) The overall transmittance as a function of λ_0 and θ for the incident wave. c) Overall transmittance and d) reflectance for all of the spatial Fourier space for $\lambda_0 = 900$ nm. e) A schematic depicting another case for incidence when all of the surrounding medium is made of silica. Panels (f), (g), and (h) analogous to (b), (c), and (d), respectively, for the schematic diagram shown in (e) ($\lambda_0 = 1100$ nm). The dashed lines correspond to the cutoff conditions of diffraction orders in the reflection and transmission domains.

evaporated on only one side of a triangular pattern as demonstrated in Figure 6b for a trial sample before oxidation (an SEM image of the investigated sample is shown in Figure S10, Supporting Information).

The measured angular dispersion of the 0th-order transmittance, for the fabricated sample of the metagrating, is shown in **Figure** 7a. The experimental measurements of the 0th-order transmittance are normalized with respect to that of a blank silicon wafer polished on both sides. It should be noted that the symmetry of the 0th-order angular transmittance is broken both in the non-diffractive and diffractive regions, which leads to a broader angular asymmetry range. Such broader range is relevant for applications where absorption is not an issue. In the non-diffractive regime, the asymmetry in transmittance exceeds 20 dB around a central wavelength of 1.1 μm. Additionally, the asymmetry of the transmission in the diffractive regime is around 8 dB over a broadband spectrum. Figure 7b shows the simulated 0th-order transmittance calculated by a finite-element solver. Note

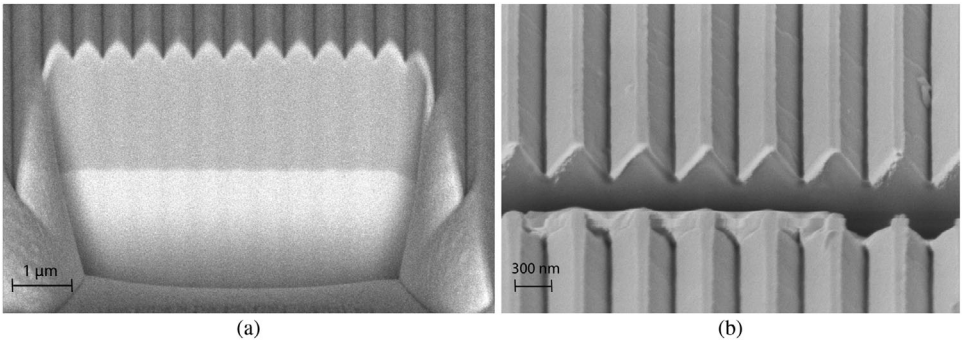

Figure 6. a) SEM image of the cross section of the fabricated triangular silica ridges after thermal oxidation. b) Same after oblique evaporation of gold on a trial sample.

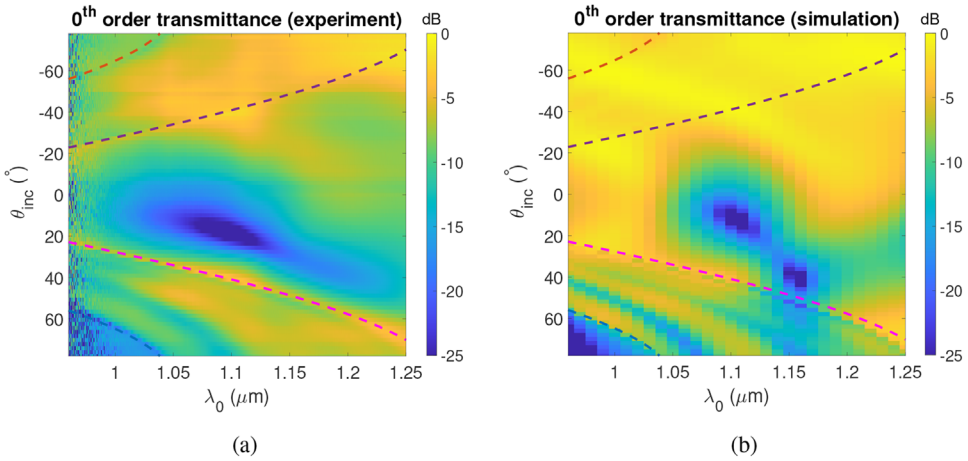

Figure 7. a) 0th-order transmittance measured by the experimental setup as a function of the incidence angle of the TM-polarized light source. b) Similar as (a) but based on full-wave simulations.

that the simulation results follow a similar trend to that of the experimental measurements in Figure 7a. However, there are some differences, particularly, in the non-diffractive regime due to fabrication imperfections and the material loss, which is not considered in the simulations. The most noticeable one is the strong dependence of the angular absorption on the curvature of the gold strips. Such curvature was observed during characterization after thermal oxidation by scanning electron microscopy (Figure S10, Supporting Information). Moreover, as it can be seen in Figure S11 (Supporting Information), the location of the transmission dip shifts remarkably for different curvature radii in the $x-$ and $z-$directions. Moreover, angular misalignment and the variations in gold and oxidation thicknesses also play a role in these differences between simulation and experiment. It is worth noting that the unit cell of the proposed metagrating cannot be simply analyzed as two separate sides where one of them is merely a mirror, while the other one is a transmissive dielectric layer. Conversely, the metagrating, as discussed earlier, could be modeled as an array of tilted dipoles which are optimized to maximize the diffraction efficiency in one particular diffraction order for both positive and negative incidence angles. This is demonstrated in Figure S12 (Supporting Information), where a unit cell covered with gold on both sides has a transmittance that ranges from 0.4 to 0.6, and does not simply behave as a mirror for both sides of incidence. Such a response stems from the fact that the gold layer's thickness is too thin to be simply regarded as a mirror, and should instead be modeled as an array of tilted dipoles. This model shows the potential of periodic systems with strong normal multipolar components (e.g., strong dipolar response along the z-direction) comparable to the tangential multipolar components (i.e., along the x-direction) for controlling the angular response of light, and paves the way for utilizing this extra degree of freedom to obtain novel functionalities. Additionally, the controllable abrupt switching from absorption to scattering by diffraction, as shown in Figure 7, could inspire future works where controllable angle-dependent absorption may be required. Furthermore, we show by full-wave simulations in Figure S14 (Supporting Information) how the metagrating's response could be shifted to the visible regime with high efficiency (i.e., the transmittance is greater than 0.9) using aluminum instead of gold.

The optical measurements were performed using a supercontinuum white light source (SuperK Extreme EXW-12 by NKT photonics), illuminating the sample, which is placed on a rotating holder. The beam is nearly collimated and is approximately 3 mm in diameter, which mimics plane-wave-like excitation. The 0th-order transmittance was recorded as a function of angle of incidence using an optical spectrum analyzer (OSA YOKOGAWA AQ6370D). A fiber coupler collects the transmitted optical signal from the sample and guides it to the OSA for spectral measurement. Since the positions of the source and fiber coupler are fixed, only the 0th order diffraction is measured in transmission, as it remains collinear with the incident beam axis after passing through the sample. Refer to the Supplementary Section 8 for the additional information regarding the optical setup.

4. Conclusion

In this work, we describe how an engineered diffractive optical system in the form of a metagrating enables a virtual knife-edge in spatial Fourier space. The metagrating can switch from transmission to reflection in an abrupt fashion, depending on the incidence angle. Such a response can find several applications in imaging and spatial computing such as achieving image filtering or a step function in Fourier space in an ultra-thin compact fashion.

Supporting Information

Supporting Information is available from the Wiley Online Library or from the author.

Acknowledgements

Open access publishing facilitated by Ecole polytechnique federale de Lausanne, as part of the Wiley - Ecole polytechnique federale de Lausanne agreement via the Consortium Of Swiss Academic Libraries.

Conflict of Interest

The authors declare no conflict of interest.

Data Availability Statement

The data that support the findings of this study are available from the corresponding author upon reasonable request.

Keywords

angular light, Fourier optics, metagratings, metasurfaces, optical computing

Received: January 23, 2025
Revised: September 5, 2025
Published online: September 25, 2025

[1] A. V. Kildishev, A. Boltasseva, V. M. Shalaev, *Science* **2013**, *339*, 1232009.
[2] H.-T. Chen, A. J. Taylor, N. Yu, *Rep. Prog. Phys.* **2016**, *79*, 076401.
[3] A. Epstein, G. V. Eleftheriades, *Phys. Rev. Lett.* **2016**, *117*, 256103.
[4] K. Achouri, O. J. Martin, *IEEE Trans. Antenn. Propag.* **2019**, *68*, 432.
[5] K. Achouri, V. Tiukuvaara, O. J. Martin, *IEEE Trans. Antenn. Propag.* **2022**, *70*, 11946.
[6] A. Momeni, H. Rajabalipanah, M. Rahmanzadeh, A. Abdolali, K. Achouri, V. S. Asadchy, R. Fleury, *IEEE Trans. Antenn. Propag.* **2021**, *69*, 7709.
[7] Y. Zhou, H. Zheng, I. I. Kravchenko, J. Valentine, *Nat. Photonics* **2020**, *14*, 316.
[8] A. Arbabi, E. Arbabi, Y. Horie, S. M. Kamali, A. Faraon, *Nat. Photonics* **2017**, *11*, 415.
[9] V. S. Asadchy, M. Albooyeh, S. N. Tcvetkova, A. Díaz-Rubio, Y. Ra'di, S. A. Tretyakov, *Phys. Rev. B* **2016**, *94*, 075142.
[10] D.-H. Kwon, S. A. Tretyakov, *Phys. Rev. B* **2017**, *96*, 085438.
[11] S. Abdollahramezani, O. Hemmatyar, A. Adibi, *Nanophotonics* **2020**, *9*, 4075.
[12] F. Zangeneh-Nejad, D. L. Sounas, A. Alù, R. Fleury, *Nat. Rev. Mater.* **2021**, *6*, 207.
[13] N. Yu, P. Genevet, M. A. Kats, F. Aieta, J.-P. Tetienne, F. Capasso, Z. Gaburro, *Science* **2011**, *334*, 333.
[14] N. Mohammadi Estakhri, A. Alu, *Phys. Rev. X* **2016**, *6*, 041008.
[15] V. Asadchy, A. Díaz-Rubio, S. Tcvetkova, D.-H. Kwon, A. Elsakka, M. Albooyeh, S. Tretyakov, *Phys. Rev. X* **2017**, *7*, 031046.
[16] F. Liu, D.-H. Kwon, S. Tretyakov, *IEEE Antennas Propag. Mag.* **2023**.
[17] A. Díaz-Rubio, S. A. Tretyakov, *IEEE Trans. Antenn. Propag.* **2021**, *69*, 6560.
[18] G. Lavigne, K. Achouri, V. S. Asadchy, S. A. Tretyakov, C. Caloz, *IEEE Trans. Antenn. Propag.* **2018**, *66*, 1321.
[19] A. Epstein, G. V. Eleftheriades, *IEEE Trans. Antenn. Propag.* **2016**, *64*, 3880.
[20] Y. Ra'di, D. L. Sounas, A. Alù, *Phys. Rev. Lett.* **2017**, *119*, 067404.
[21] Y. Ra'di, A. Alù, *IEEE Photonics J.* **2021**, *14*, 1.
[22] T. Davis, F. Eftekhari, D. Gómez, A. Roberts, *Phys. Rev. Lett.* **2019**, *123*, 013901.
[23] H. Fan, J. Li, Y. Lai, J. Luo, *Phys. Rev. Appl.* **2021**, *16*, 044064.
[24] X. Wang, A. Díaz-Rubio, V. S. Asadchy, G. Ptitcyn, A. A. Generalov, J. Ala-Laurinaho, S. A. Tretyakov, *Phys. Rev. Lett.* **2018**, *121*, 256802.
[25] H. Rajabalipanah, A. Momeni, M. Rahmanzadeh, A. Abdolali, R. Fleury, *Nanophotonics* **2022**, *11*, 1561.
[26] A. Cordaro, B. Edwards, V. Nikkhah, A. Alù, N. Engheta, A. Polman, *Nat. Nanotechnol.* **2023**, 1.
[27] N. V. Golovastikov, D. A. Bykov, L. L. Doskolovich, *Opt. Lett.* **2015**, *40*, 3492.
[28] C. Xu, Y. Wang, C. Zhang, B. Dagens, X. Zhang, *Opt. Lett.* **2021**, *46*, 4418.
[29] Y. Zhou, J. Zhan, Z. Xu, Y. Shao, Y. Wang, Y. Dang, S. Zhang, Y. Ma, *Laser Photonics Rev.* **2023**, *17*, 2300182.
[30] E. Sakr, S. Dhaka, P. Bermel, in *Physics, Simulation, and Photonic Engineering of Photovoltaic Devices V*, vol. *9743*, SPIE **2016**, pp. 217–224.
[31] L. Duempelmann, D. Casari, A. Luu-Dinh, B. Gallinet, L. Novotny, *ACS nano* **2015**, *9*, 12383.
[32] It may also be achieved with a structure with fully broken symmetry at the cost of a more complicated fabrication procedure.
[33] A. Overvig, A. Alù, *Laser Photonics Rev.* **2022**, *16*, 2100633.
[34] K. Shastri, F. Monticone, *Nat. Photonics* **2023**, *17*, 36.
[35] G. Schmidt, *Appl. Math.* **2013**, *58*, 279.